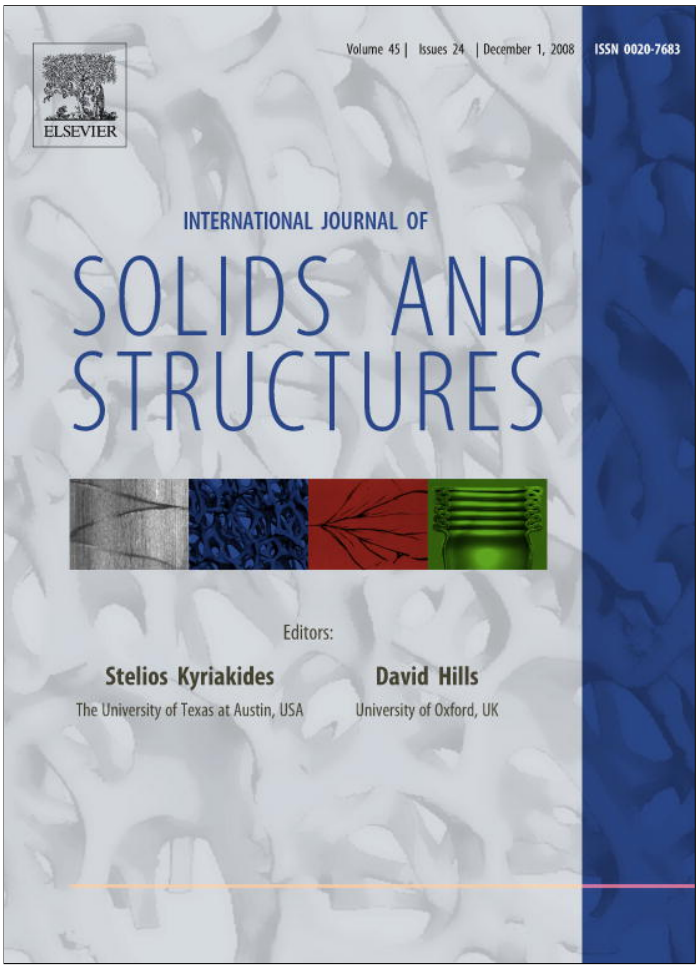

International Journal of Solids and Structures 45 (2008) 6190–6204

Contents lists available at ScienceDirect

International Journal of Solids and Structures

journal homepage: www.elsevier.com/locate/ijsolstr

Compliant multistable structural elements

M. Santer [a,*], S. Pellegrino [b]

[a] Department of Aeronautics, Imperial College London, Prince Consort Road, London SW7 2AZ, UK
[b] California Institute of Technology, 1200 East California Boulevard, Pasadena, CA 91125, USA

ARTICLE INFO

Article history:
Received 17 January 2008
Received in revised form 30 May 2008
Available online 31 July 2008

Keywords:
Adaptive structure
Bistable structure
Compliant structure

ABSTRACT

Compliant multistable structures are presented which exhibit a large geometric change when actuated between their stable states. It is demonstrated how asymmetric-bistability is achieved through the combination of linear and nonlinear springs. Finite element analytical techniques are provided which enable the design of such structures, and which illustrate how the presence of imperfections can substantially alter their structural performance. A multistable structure is developed which consists of four connected bistable tetrahedral units. The validity of the analytical techniques is confirmed through observation of several physical models.

1. Introduction

In this paper, the aim is to illustrate the design of a compliant *bistable* structural element which is then incorporated with a number of similar elements. This results in a structure which has a large number of discrete stable configurations and which may be utilised as a *multistable* adaptive structure. The structural elements are intended to be asymmetrically-bistable; in other words they have one stable state which has a greater amount of stored strain energy and is therefore less energetically-preferential than the other stable state.

A compliant structure is one in which the functionality provided by conventional mechanism components, such as rotational hinges, is provided by the elastic flexure of elements within the structure itself (Howell, 2001). For example, the compliant equivalent to the rotational hinge is a thin beam subject to bending, known as a compliant or living hinge. Compliant structures have a number of advantages over conventional mechanisms.

Of these advantages, one of the most important is the possibility to reduce the number of components necessary to perform a particular function. In the case of a conventional rotational hinge, at least three components – two rotating elements and a connecting pin – are required. These must be assembled, which adds to the complexity of the manufacturing process. In contrast, a living hinge is simply an area of a structure with increased flexural compliance, achieved by localised thinning, and may be fabricated in the same process as the remainder of the structure. In addition, the absence of sliding between adjacent parts means that compliant structures may be more suited to environments which are not suited to mechanisms, for example outer space where the phenomenon of out-gassing prevents the use of several lubricants.

Structures which are in stable equilibrium in more than one distinct geometric configuration may be used as adaptive structures. The majority of structures are intended to remain in the same configuration throughout their design lifetime. However, an adaptive structure may change its configuration, usually by means of embedded actuation. This enables it to have more than one equilibrium configuration. If the adaptive structure is also multistable, it will remain in its new configuration even when power to the actuators is removed. This is particularly useful if the structure is intended to remain in its alternative configurations for a long time.

* Corresponding author. Tel.: +44 20 7594 5117.
E-mail address: m.santer@imperial.ac.uk (M. Santer).

0020-7683/$ - see front matter © 2008 Elsevier Ltd. All rights reserved.
doi:10.1016/j.ijsolstr.2008.07.014

When multistable structures are also compliant structures the advantages of both are retained. In this paper, the focus is on the design of compliant bistable structures. These bistable structures may then be connected to form a multistable structure. As shown by Chirikjian, 1994, a multistable structure consisting of n distinct bistable elements possesses a maximum of 2^n discrete stable states.

The outline of the paper is as follows. First, a definition of asymmetric-bistability is provided. The implications of designing such a structure are discussed. All of the structures that are presented in this paper are formed from combinations of linear and nonlinear spring elements. How this leads to asymmetrically-bistable behaviour will be demonstrated.

Examples of three-dimensional structural elements based around combinations of linear and nonlinear springs are then presented. It is demonstrated that, depending on the initial geometry and the presence of imperfections, many stable states may be present and undesired buckling modes may be observed. This is then used to develop a design for an element which is truly bistable and imperfection insensitive. Finally, a multistable structure consisting of four connected asymmetrically-bistable structures is demonstrated.

2. Asymmetric-bistability

Bistable structures have total potential energy functions with two distinct potential wells separated by an unstable potential hill. When an actuator is required to cause the bistable structure to switch between the stable states, it is necessary for sufficient energy to be imparted to the structure by the actuator. This energy has to bring the structure out of its current potential well and traverse the crest of the potential hill. At this point, the bistable structure will continue to change its configuration to the second stable state unassisted, as this represents the path of least resistance.

2.1. Definitions of symmetric-bistability

Symmetric-bistability case occurs when the structure has equal stored strain energy in the two stable states. The total potential energy profile for a range of configurations of a typical symmetrically-bistable structure is shown in Fig. 1, and can be seen that the stable states S_1 and S_2 have the same potential, but there is no requirement in the definition for the structure to be equally stiff in both stable configurations.

An *asymmetrically-bistable* structure is defined as one in which one of the two stable configurations has a higher total potential energy than the other. A typical potential energy profile for a range of configurations for an asymmetrically-bistable structure is shown in Fig. 2. In this case, the stable state S_1 has a total potential energy that is ΔU higher than the second stable state S_2. This means that the structure has a preferred stable state corresponding to the lower potential energy value.

2.2. Effects of symmetric-bistability

Having provided a definition of symmetric- and asymmetric-bistability, we now consider the general actuation requirements of the two types of bistable structure. Considering first the symmetrically-bistable case (as shown in Fig. 1) it can be seen that in order to cause the structure to change configuration from the first to the second stable state (S_1 to S_2), the actuator must do sufficient work to move the structure out of the potential well, i.e. to raise U from S_1 to the unstable point B at which point the structure will snap to the second stable configuration S_2.

If we consider bistable structures that are designed to be integrated into multistable structures that have practical use, it is likely that when the structure changes configuration there will be a requirement for work to be done, such as working against gravity or lifting a load. This work must be provided by the actuator in addition to the work required to raise the potential energy of the structure from S_1 to point B. After this point as the structure transitions to the stable state S_2 the potential energy input may be released as useful work and the driving actuator is no longer required. This release of potential

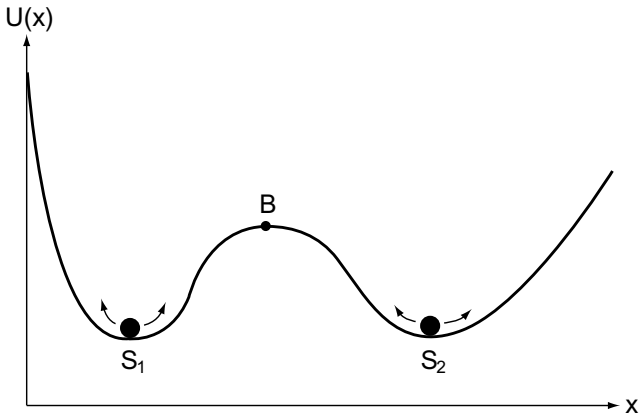

Fig. 1. Indicative energy U vs. configuration x plot for a structure that is symmetrically-bistable.

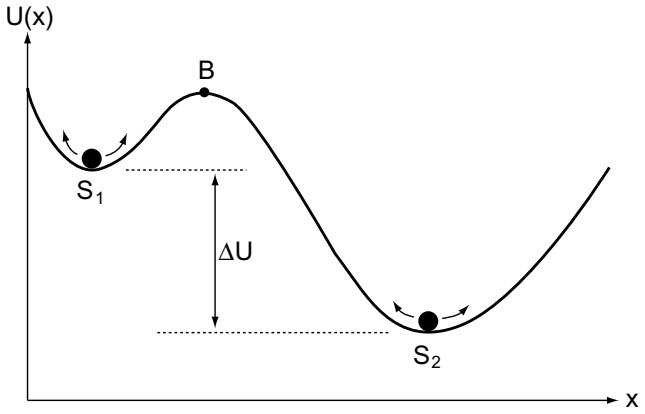

Fig. 2. Indicative energy U vs. configuration x plot for a structure that is asymmetrically-bistable.

energy in a dynamic snap-through typically occurs much more quickly than energy can be released by the majority of currently available actuator technologies.

The same is true for asymmetrically-bistable structures, but in this case the amount of work the actuator must input in order to raise U from S_1 to B, is considerably less than the amount of work that will be rapidly released when the structure transitions from B to S_2. This means that if a rapid rate of work release (high power output) is required during the change of structural configuration it can be beneficial to choose an asymmetrically-bistable structure as the basis.

However, the actuation of the return transition from S_2 to S_1 is also affected by the symmetry of the bistable structure. In the case of a symmetrically-bistable structure the work input by the return actuator is exactly the same as required by the driving actuator, so the actuator requirements for both are likely to be similar. For asymmetrically-bistable structures the returning actuator has to do ΔU more work than the driving actuator, which would appear to place an undesirable burden on the selection of a suitable actuator. However, if there is no need for a high speed transition in the return direction then the energy can be pumped into the system slowly.

It is worth noting that with both types of bistable structure, the accuracy of a change in configuration may be controlled by the structure itself rather than by the precision of the driving actuators (Plante et al., 2005). This does, however, place certain requirements on the actuators, for example that they should have low stiffness, or be of a unilateral kind.

2.3. Achieving asymmetric-bistability

It can be seen in Fig. 3(a) that when two linear springs are paired the resulting structure can never be bistable as the equilibrium paths of each spring may only cross at one point. When one linear spring is replaced with a nonlinear spring, bistable structures may result if it is possible for the equilibrium paths to cross more than once. This guarantees at least two equilibria, although their stability needs to be assessed through further investigation. This is sketched in Fig. 3(b).

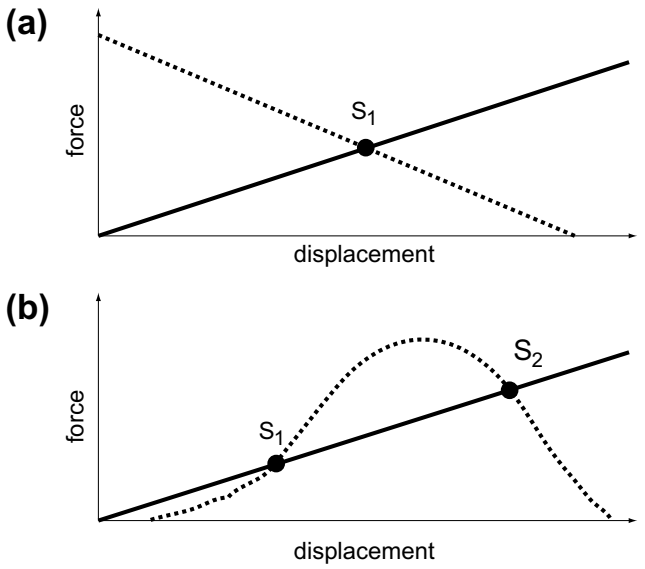

Fig. 3. (i) Force vs. displacement plots for two paired linear springs indicating the single possible equilibrium configuration. (ii) Force vs. displacement plots for a paired linear spring and nonlinear spring indicating the possibility of additional equilibrium configurations and hence structural bistability.

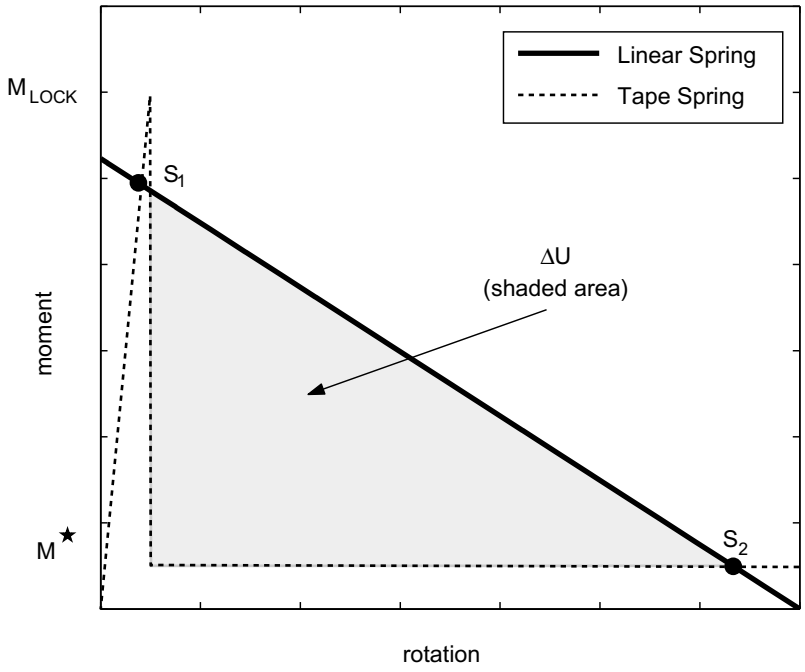

Fig. 4. Moment vs. rotation plot for a coupled linear and nonlinear (tape) spring. S_1 and S_2 are stable equilibrium configurations.

The nonlinear springs that are used for the bistable elements discussed in this paper are tape springs. A tape spring is a beam-like element with a curved cross-section that exhibits limit-point buckling on application of a critical bending moment (Seffen and Pellegrino, 1999). Its moment–rotation properties are largely independent of length and its geometry may be characterised in terms of the radius of curvature R and the subtended angle α of the cross-section. Up to this critical moment M_{LOCK} the tape spring responds as a beam exhibiting a high stiffness and an approximately linear moment–rotation relationship. Following buckling however, the tape spring continues to exert a reduced bending moment, denoted $M^{\star}$, which may be considered approximately constant for design purposes.

The moment–rotation behaviour for a spring with a linear response coupled with a tape spring, having the idealised response described above, is sketched in Fig. 4. As the behaviour plotted in Fig. 4 is fundamental to the understanding of how asymmetrically bistable behaviour is achieved, it is worthwhile to discuss it in some detail.

As we move from left to right, we can see that the tape spring is moving from straight and unbuckled, and hence exhibiting an approximately linear response, to buckled and exerting an approximately constant restoring moment. At the extreme left hand side, the tape spring is straight and the linear leaf spring is curved (the response shown with an unbroken line) and exerts a restoring moment. Provided this moment is less than the critical tape spring buckling moment M_{LOCK} this results in a stable equilibrium at the point marked S_1. When a sufficiently large moment is applied such that its value in combination with the linear spring moment exceeds the tape spring critical value M_{LOCK}, the structure then snaps through to the second equilibrium point S_2 which represents the point at which the moment exerted by the leaf spring is in equilibrium with the tape spring moment $M^{\star}$. The stored strain energy, corresponding to ΔU in Fig. 2, is represented by the shaded area bounded by the equilibrium curves. It is this energy which may be released as useful work over the transition above that provided by the driving actuator, and which must be pumped back into the system by the actuators resetting the structure to its initial configuration.

3. Asymmetrically-bistable tetrahedral elements

In this section, a three-dimensional structural element concept, based around the pairing of linear springs and nonlinear tape springs described in Section 2.3, will be introduced. To construct these elements, two tape springs are orientated at 90° to each other so that their end points meet at the vertices of a geometric tetrahedron. The tape springs are then connected to each other by slender elastic rods. These rods are chosen to have a circular cross-section in order to limit orientation effects and to provide greater ease of design. These elements are likely to be subjected to twist in addition to bending during the transition between stable states.

The connection between the tape springs and the slender rods is provided by connection pieces. These pieces provide many useful functions, including providing an attachment point for actuators, and to form connections between adjacent multistable tetrahedra if several are integrated into a multistable system. However, one of their most useful features is that they provide a large amount of design freedom, in particular by allowing the rod ends to be offset from the tape spring ends. Of course such an offset may result as an imperfection from the manufacturing as well as being included as an intentional

design variable. The variation of this offset is illustrated in Fig. 5. Fig. 5(a) shows the slender rods in a multistable tetrahedral structure with zero offset in their straight configuration. Tape springs are not shown, but are assumed to connect points 1 and 2, and points 3 and 4. The angle β between adjacent rods is the same at all four points.

In order to limit the scope of the design, we restrict ourselves to the consideration of structures in which the offset lies between: zero, shown in Fig. 5(a), and in which case the rods meet at a point resulting in a fully triangulated structure; and the case in which the rods are parallel and $\beta = 0$, shown in Fig. 5(b). We also consider the configurations that are of greatest interest to be those that maximise the change in a chosen geometric parameter between the stable states, for example the change in height h as defined in Fig. 5(a) or enclosed volume.

It should be noted at this point that even when the rod offset is large, the structures are still considered to be multistable tetrahedra, although their resemblance to the geometric solid becomes rather remote. Hence, any multistable structure in which tape springs connect points 1 and 2, and 3 and 4, which form the vertices of a geometric tetrahedron, is referred to as a 'multistable tetrahedron'.

It was chosen to set up the tetrahedra in their low-energy stable configuration, i.e. with both tape springs bent. This enabled the tetrahedra to be constructed in a configuration in which the rods are initially straight. Clearly after fabrication there will be some initial deformation while the rods deform to equilibrate the bent tape springs' constant resisting moment $M^{\star}$. The method of effecting the transition between the stable states is to apply opening moments M to the ends of the tape springs, as shown in Fig. 6. The structure is the same as shown in Fig. 5(a) except the tape springs are also shown. These moments must be sufficient to deform the rods into the high-energy stable configuration. For this new configuration to be stable, the rods in their deformed configuration must exert a moment on the tape springs less than the critical tape spring moment M_{LOCK}. If a particular tetrahedron design is bistable, on removal of the actuation moments, the structure will remain in its new configuration.

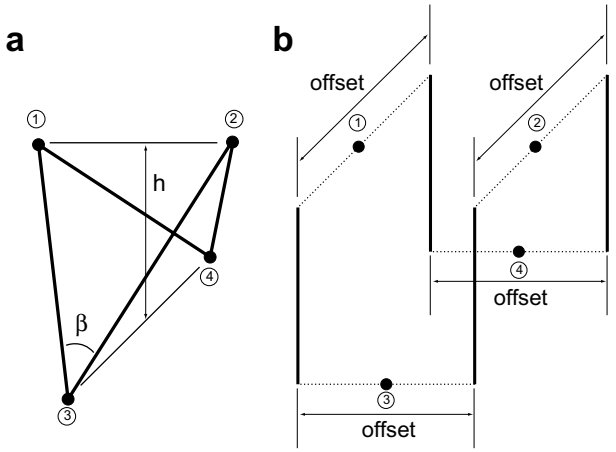

Fig. 5. Illustration of rod end offset in multistable tetrahedron. (a) Slender rods arranged in a zero-offset configuration. (b) Slender rods having maximum permissible offset such that they are parallel.

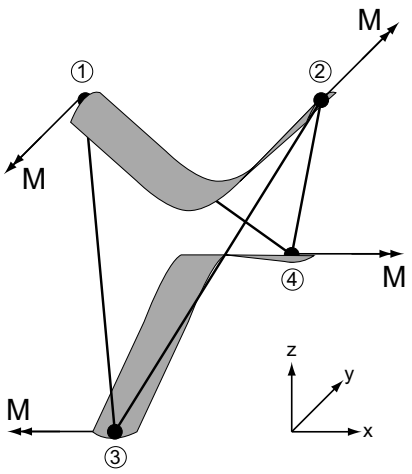

Fig. 6. Actuation moments M applied to cause the transition between the stable states of a bistable tetrahedron.

3.1. Analysis

In this section, we describe the several analysis techniques that are used to characterise the behaviour of multistable tetrahedra. The initial stage of the design process is to ensure that the tetrahedron *can* possess two stable states, one in which both tape springs are bent, and one in which both tape springs are locked, and to then determine the geometrical configurations of these stable states. This requires a knowledge of the restoring moments that are produced when the slender rods are deflected.

3.1.1. Rod and tape spring matching

The first stage of the design process is to decide the configuration that the straight rods will have, and their initial length a. Initially the moments resulting from end-rotations of the rods were analysed using linear standard-cases. It was found, however, that for all but a small minority of possible geometries, this was not a suitable approach as the displacements are usually large.

Instead, an ABAQUS v.6.7-1 finite element model of the rods in this configuration is constructed. The slender rods are initially modelled using B31 Timoshenko beam elements. The beam elements are assigned isotropic material properties representative of carbon-fibre reinforced polymer (CFRP): Young's modulus $E = 134\,\mathrm{N/mm^2}$, and a Poisson's ratio of 0.4. A large number of beam elements is used per rod, as the deflections are large. An example of a finite element mesh for a 'perfect' tetrahedral structure is shown in Fig. 7. In this example, 50 beam elements are defined per rod. Boundary conditions are applied to points 1, 2, 3 and 4. Points 1 and 2 are constrained against displacement in the y-direction. Points 3 and 4 are constrained against displacement in the x- and z-directions Note that the tape springs are not included in this model. By setting known displacements δ and rotations θ on the four corner points of the finite element model, we can determine the tape spring requirements in terms of the moments $M^\star$ and M_{LOCK} and the length b.

First $M^\star$ is determined. It is desirable for the difference between M_{LOCK} and $M^\star$ to be as large as possible in order to maximise the stored strain energy difference ΔU between the two stable states. This means that $M^\star$ should be as small as possible, and the corresponding stable state should allow the rods to remain in a configuration as close to straight as possible. An allowable rotation θ is applied in the FE analysis and the corresponding reaction moment provides a value for $M^\star$. For small deflections, it is sufficient to approximate the applied displacement as $\delta = 0$. In all the designs presented in this paper, the action of $M^\star$ resulted in a maximum rotation of $\theta = 10^\circ$.

To determine a value for M_{LOCK} it is necessary to choose a tape spring length b. If b is relatively long, it can result in an increase of the change in height h between stable configurations, at the expense of increasing the required value of M_{LOCK}. In the rod FE model, the displacement $\delta = (b - L_0)/2$, and the rotation $\theta = \theta_{\max}$ necessary to allow the tape springs to adopt a straight, locked configuration are applied to each of the four vertex points. The corresponding reaction moment provides a value for M_{LOCK}.

Having determined values for the required tape spring moments, a suitable cross-section geometry must be found. This is carried out by means of a further finite element analysis. The tape springs are modelled using quadrilateral S4R shell elements having reduced integration and a large strain formulation. The material properties were assumed to be those determined by Dano et al., 2000 for triaxial-weave CFRP, i.e. orthotropic with $E_{11} = 31,000\,\mathrm{N/mm^2}$, $E_{22} = 22,300\,\mathrm{N/mm^2}$, $G_{66} = 3050\,\mathrm{N/mm^2}$, and $\nu_{12} = 0.58$. The cross-section thickness is 0.15 mm, but this was reduced in the analysis by 40%

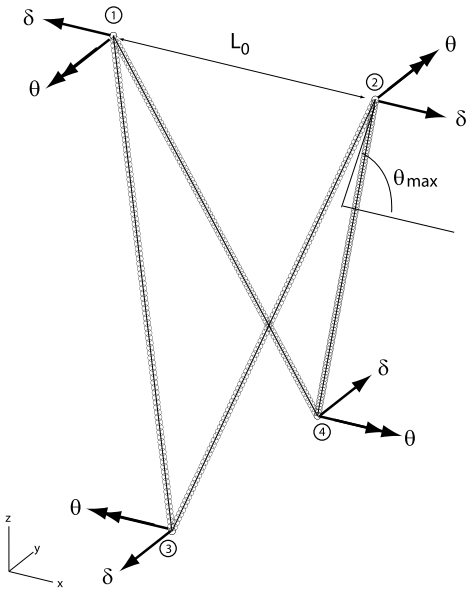

Fig. 7. End displacements and rotations applied to a finite element model of the slender rods used to determine the required tape spring properties.

to 0.09 mm to account for the reduction in second moment of area of the cross-section due to the packing of the fibres in the weave.

When the rod end offset is introduced as a design variable, an infinite number of potential initial tetrahedron configurations may be achieved. In all cases suitable tape spring geometries may be matched to the desired rod configurations by means of the above method. In order to investigate the stability of the multistable tetrahedra more closely, two examples will be considered in detail. It will be shown that the initial as-constructed configuration has a strong influence on the predicted and observed behaviour of the tetrahedra.

The two tetrahedra that are investigated are shown in their 'as-constructed' state in Fig. 8. Tetrahedron A has partially bent tape springs, and rods that have zero end offset. Tetrahedron B has tape springs bent through 180° and rods having sufficient end offset to make them initially parallel. The precise geometries of tetrahedra A and B are tabulated in Table 1.

3.1.2. Modelling of bistable tetrahedra using ABAQUS

The construction of the FE model closely followed the construction of the physical models. First, an analysis of the tape springs, not attached to any other structure, was carried out in which the tape springs were deformed into the configuration required to fit with the rods in their initial configuration. The tape springs in their stressed, deformed configuration were then incorporated with the unstressed rods by means of the ABAQUS *IMPORT function. The connection pieces between the rods and the tape springs are modelled as multi-point constraints (MPCs) which fully restrain all relative translations and rotations.

3.1.2.1. Verification of stable equilibrium configurations. The first step of the analysis is to confirm that the tape springs have been correctly matched to the rods, and that the structure can be in equilibrium with both tape springs locked, or both tape springs unlocked. This is carried out by initially allowing the model to relax into the low-energy stable state with both tape springs bent. This is achieved with an analysis step in which boundary conditions identical to those described in Section 3.1.1 are applied, with no loading. This allows the structure to adopt its new equilibrium configuration.

Next, the ends of one of the tape springs are fixed and opening moments sufficient to straighten the other tape spring are applied to its ends. When this tape spring has straightened all applied loads are removed and a relaxation step is used to ensure that the new configuration is stable. The same procedure is applied to the other tape spring, at which point the structure is allowed to relax by maintaining the boundary conditions and removing all external loads in a new analysis step. Stable states for Tetrahedron A are shown in Fig. 9.

States (a) and (c) are the predicted stable configurations. Because the tape springs are opened in sequence, rather than simultaneously, additional stable equilibrium configurations are obtained. One of these intermediate states is shown in Fig. 9(b). There is an identical stable state in which the configuration of the two tape springs is reversed. Hence, the structure has four stable equilibrium states.

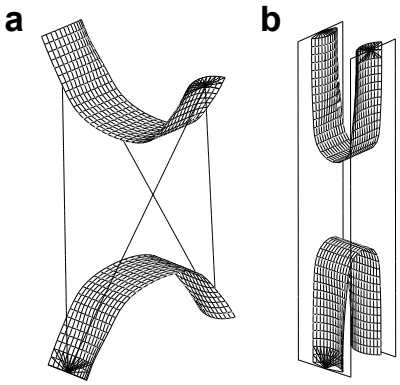

Fig. 8. FE models of two example multistable tetrahedra in their pre-relaxed configurations. (a) Tetrahedron A. (b) Tetrahedron B.

Table 1
Defining characteristics for Tetrahedron A and Tetrahedron B

	Tetrahedron A	Tetrahedron B
Rod length, a	100 mm	100 mm
Tape spring length, b	80 mm	80 mm
Rod offset	0	20 mm
Rod angle, β	30°	0
Tape spring radius, R	8 mm	8 mm
Tape spring subtended angle, α	90°	90°
Mass	2 g	2 g

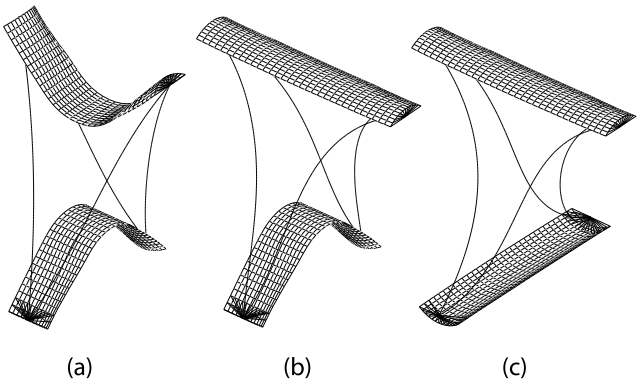

Fig. 9. FEA predictions of the stable equilibrium configurations of Tetrahedron A.

Tetrahedron B exhibited a different response. On release from the as-constructed configuration, the structure adopted the predicted low-energy stable state in which both tape springs are bent. This state is shown in Fig. 10. When it was attempted to verify the additional stable configurations by relaxation, however, the analysis failed to converge. In ABAQUS, this can be indicative of model instability.

3.1.2.2. Stability along the transformation path. When the stability of a structure is assessed, an eigenvalue analysis in its initial, i.e. un-deformed, configuration is usually sufficient. Hence, the stability of Tetrahedra A and B when subject to a gradually increasing opening moment M was investigated using the ABAQUS *BUCKLE eigenvalue buckling analysis. This initial analysis was carried out for the structures in the low-energy stable configuration that is obtained by allowing the as-constructed configuration to relax. For both tetrahedra, the critical moment M_{CRIT} were found to be substantially lower than the moments required to straighten the tape spring, which would appear to indicate that the equilibrium configurations shown in Fig. 9(b) and (c) are in fact unstable. This was an unexpected result, and so a more refined analysis of the stability along the transformation path was carried out.

A buckling analysis is performed initially in the low-energy stable state to estimate the first critical moment M_{CRIT}. The structure was then subject to an opening moment, M, set at a value below the previously calculated M_{CRIT}, then the new equilibrium configuration was found, and then the critical moment was re-estimated. This process was continued until the applied opening moment was sufficient to straighten the tape spring.

This analysis was repeated for three different examples, Tetrahedra A and B and an additional tetrahedron, referred to as Tetrahedron C, which has the same initial tape spring bending and relative positioning as Tetrahedron A but with the rods offset to make them parallel. For all these examples M_{CRIT} always remains higher than M, and consequently the structures do not buckle.

It transpires that the behaviour of the critical moment associated with the first *torsional buckling mode* M_{TOR} is, however, particularly significant. Therefore, the value of $M_{TOR} - M$ with M is plotted for values of M up to 20 N mm which is sufficient to straighten the tape spring, in Fig. 11. When $M_{TOR} - M = 0$ the structure will buckle into a torsional mode. For all examples, the torsional model greatly reduces from its initial value when the structure is transitioned between stable states. For Tetrahedra A and C, after this initial reduction, there is substantially less variation in M_{TOR} over the remainder of the transition, until the second stable state is reached and it climbs again. Tetrahedron B, however behaves in a different way – the torsional buckling moment decreases relative to the applied moment throughout the transition until $(M_{TOR} - M)$ reaches the small value of 2.4 Nmm. Although this is close to zero, M_{TOR} remains greater than the applied moment at all points during the tran-

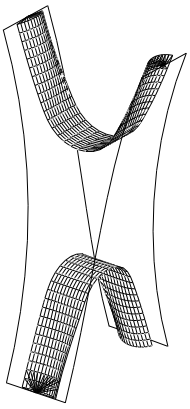

Fig. 10. FEA prediction of the low-energy stable equilibrium configuration of Tetrahedron B.

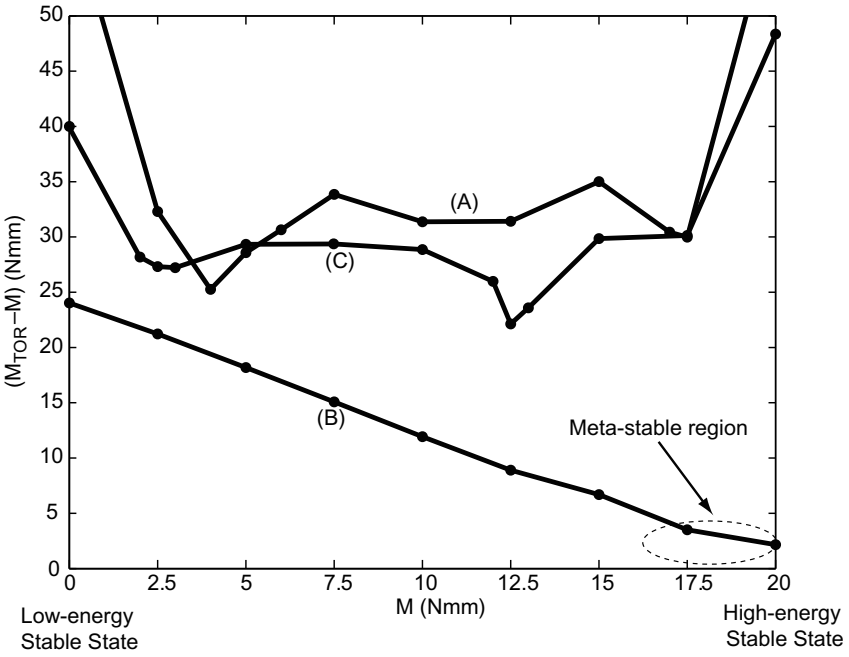

Fig. 11. A plot showing the effect of opening moment M on the critical torsional moment M_{TOR}.

sition. This close proximity of M_{TOR} to the applied moment, and hence the proximity of the structure to buckling into a torsional mode, is of interest and is investigated further.

3.1.2.3. Torsional stability. An analysis of the stability of the torsional mode was then carried out, having applied a small imperfection consisting of two opposite torsional couples. Each couple is applied through small, fictitious trigger loads, Fig. 12(a). The multistable tetrahedron is shown from the top.

For very small trigger loads the response is unchanged to that plotted in Fig. 11, $M_{TOR} - M$ always remains greater than the applied moment, but for a sufficiently large value (in the case of Tetrahedron B equal to 0.2 N at each end) $M_{TOR} - M \to 0$ which indicates that torsional instability will occur. This tendency is shown in Fig. 12(b). In this case the solid curve was generated up to the point at which the FE analysis was unable to converge. The analysis was then continued by means of an arc-length-based method (using the ABAQUS *STATIC, RIKS command) which shows large torsional deflection at a constant opening moment of 15.9 N mm. This result suggests that a torsional imperfection leads to an unstable post-buckling path. This means that Tetrahedron B has a meta-stable configuration, i.e. a configuration that is mathematically stable, but can become unstable due to small additional imperfections – in this case simulated by the addition of trigger loading.

To model what happens once the torsional instability has been triggered requires a model that includes the effects of physical contact between the rods. A central section (one third of the total length) of each rod – previously modelled with

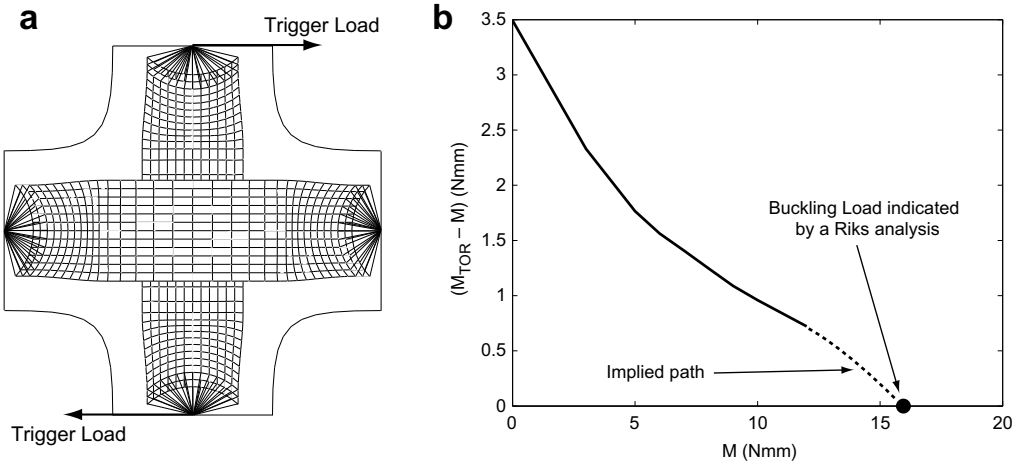

Fig. 12. Effect of the introduction of a torsional imperfection. (a) FE model showing the application of torsional trigger loading to a tape spring. (b) The effect of opening moment M on the critical torsional moment MTOR when trigger loading is included.

Timoshenko B31 elements – is replaced with C3D8R brick elements with the outside face of the cylinder being defined as contact surfaces using *CONTACT. The structure was then subject to the same trigger loads which in the previous analysis had instigated the torsional instability. When one tape spring rotates sufficiently relative to the other, the rods come into contact. This has the effect of increasing the torsional stiffness of the structure and thus preventing further rotation. Fig. 13(a) and (b) show the structure just before and after this contact, respectively. It has not currently proved possible to achieve full convergence of the FE solution in a torsionally distorted configuration, although these shapes have been observed in physical models.

3.2. Physical models

Physical models of Tetrahedron A and Tetrahedron B were constructed to verify the analysis. The tape springs were made from a single ply of triaxial-weave CFRP. The slender rods were pultruded carbon rods having the required circular cross-section and a diameter of 0.030 in. (0.762 mm). The corner pieces were constructed from a stiff acrylic plastic, and had curved faces to match the chosen tape spring geometry, and holes to locate the rods correctly. These parts were glued using cyanoacrylate adhesive.

A physical model of Tetrahedron A is shown in Fig. 14(a) in three of its four stable equilibrium configurations (remember that there are two intermediate stable states, where either one of the tape springs is locked while the other is straight). Fig. 14(b) shows the stable states predicted by an ABAQUS analysis, seen from the same orientation for comparison. It can be seen that in the low-energy stable state, the bend in the tape spring is less than predicted. This is because $M^{\star}$ is underestimated due to the inaccuracies of the smeared orthotropic approximation to the tape spring material properties. The generic behaviour is, however, identical.

The physical model of Tetrahedron B exhibited the analytically-predicted low-energy stable state. A photograph comparing the model with the analytical model in this state is shown in Fig. 15.

The imperfections in this model are sufficient to cause it to become torsionally unstable before the desired high-energy stable state is reached. When one of the tape springs has revolved by just under 180°, contact between the rods causes the structure to regain positive stiffness and reach the second stable state, shown in Fig. 16(a). From this point, the tetrahedron is able to assume higher energy stable configurations that are similar to those shown in Fig. 14. These additional stable states are shown in Fig. 16(b) and (c). Once again, state (b) represents a pair of additional stable states as the structure is stable when either one of the tape springs is bent while the other is straight.

3.3. Design of a truly bistable tetrahedron

The tetrahedra that have been presented so far have exhibited a minimum of four distinct stable states (in the case of Tetrahedron A). The primary goal of the design of the tetrahedra however is to produce an asymmetrically-bistable structure that could be incorporated into a multistable system, as discussed in Section 1. It is recognised that Tetrahedron A could be made functionally bistable by actuation (i.e. ensuring that the intermediate states are always traversed) but this is not a good solution. One of the primary benefits of using bistable structures as the basis of multistable systems is that the bistable element may only be in one of two configurations. If the configuration of each bistable component is known, the configuration adopted by the complete multistable system may be inferred. If an actuator fails mid-way through a transition there can be no certainty about the configuration that the tetrahedron has adopted.

A refinement to the basic tetrahedron concept is proposed in which, in the low-energy state, the tape springs are passed over each other and connected by slender rods in a fully triangulated configuration. Following the observation of the post-buckled behaviour of Tetrahedron B – that internal contact can be used to impart additional stiffness to a structure – the

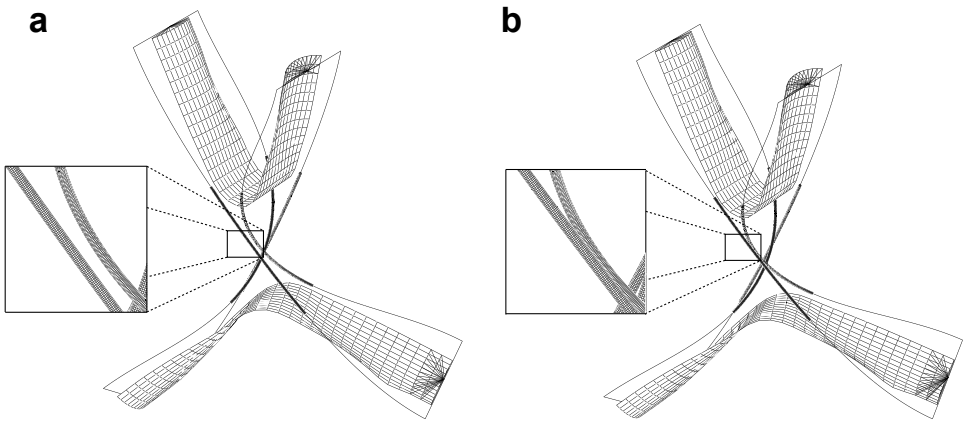

Fig. 13. FEA demonstrating rod contact in the torsional post-buckling regime. (a) Prior to rod contact. (b) Post rod contact.

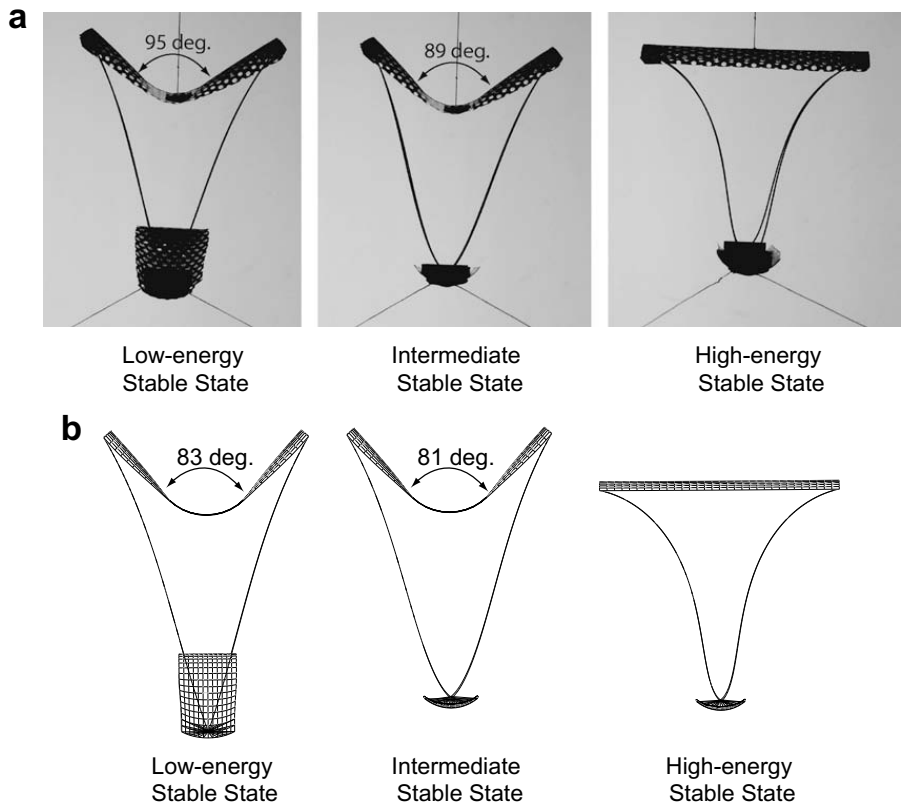

Fig. 14. Three stable states of multi-stable Tetrahedron A: physical model compared to analytical predictions. (a) Stable equilibrium configurations of the physical model of Tetrahedron A. (b) Stable equilibrium configurations as predicted by the analytical model of Tetrahedron A.

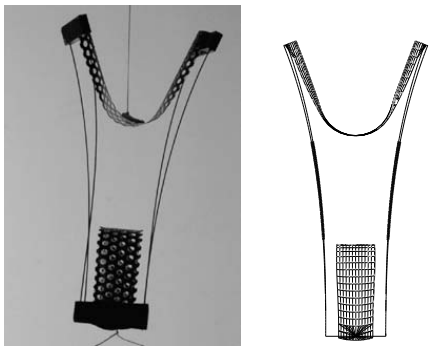

Fig. 15. The low-energy stable state of Tetrahedron B as observed and predicted.

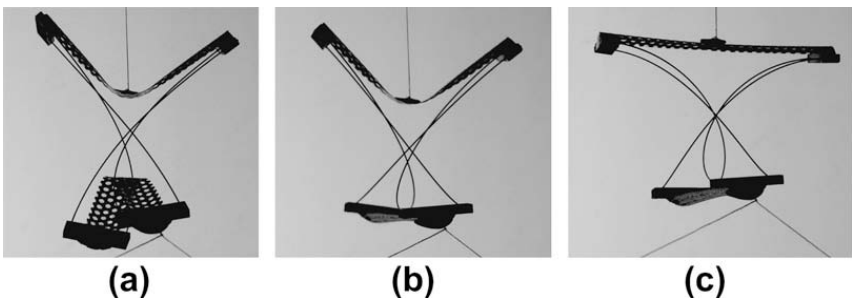

Fig. 16. The stable equilibrium configurations of Tetrahedron B following buckling into a torsional mode.

purpose of passing the tape springs around each other is that when only one tape spring is straightened, there is contact between the midpoints of both tape springs. This contact means that the intermediate stable states, where one tape spring

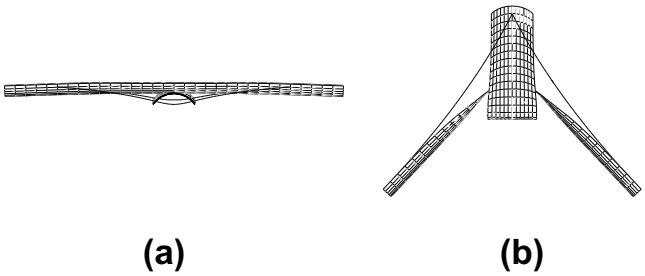

Fig. 17. Analytical predictions for the stable states of a truly bistable tetrahedron.

Fig. 18. Photographs of the stable states of a truly bistable tetrahedron model.

is straight and the other bent, are no longer possible. When both tape springs are fully straightened, the tetrahedron is in a stable high-energy configuration.

The results of an FE analysis, in which a contact surface was defined between the two tape springs, are that the two stable states for the tetrahedron are as shown in Fig. 17. It was verified by means of the procedure described in Section 3.1.2 that there are no intermediate stable states for this design.

The analytical predictions are confirmed by comparison to a physical model. Photographs of this model in the two stable states, which may be compared to those shown in Fig. 17, are shown in Fig. 18. The physical model illustrates that the tetrahedron is indeed genuinely bistable. It will be noted, however, that the photograph of the high-energy stable state, Fig. 18(a), shows local distortion of the tape springs where the slender rods are braced against their edges. This is undesirable but an easily applied refinement to the design would be to remove material from the tape springs locally at the points of contact. This would have no major effect on the performance of the tetrahedron, as the tape spring folds are localised at the centres.

4. Multistable super-tetrahedron structure

4.1. Tetrahedron-based binary robotic system

In this section a multistable system based around four bistable tetrahedral elements is demonstrated. The resulting structure exhibits a number of desirable features. This includes a substantial increase in height and enclosed volume when all the bistable elements are actuated from their high-energy to their low-energy stable states. These large changes in geometric configuration are achieved using compliance without the need to use conventional mechanism components. The structure is also very lightweight.

The method that is adopted to link bistable units together to form multistable systems is to consider the bistable structure as a rigid entity and to consider ways in which many may be assembled with spherical joints to form larger structures that are both statically-determinate and kinematically-determinate. Static determinacy means that each individual rigid element in the system may change its configuration without inducing stress in any of the other elements in the system; kinematic determinacy means that the system will have a defined configuration for every possible combination of states of the individual elements. This may be done with a mobility analysis Hunt, 1978, which is a generalisation of Maxwell's equation. If the mobility $\mathscr{M}$, which is an expression of the number of degrees of freedom, of a proposed assembly corresponds to the number of rigid-body modes, it may be a suitable candidate for use as the basis of a multistable system. The static and kinematic determinacy may be assessed by inspection.

An assembly known as a super-tetrahedron is proposed, i.e. a tetrahedron consisting of four small tetrahedral elements connected by spherical joints. The super-tetrahedron may be confirmed by a mobility analysis to be statically- and kinematically-determinate and consequently a suitable candidate for a binary robotic system. The bistable tetrahedron presented in Section 3.3 and shown in Fig. 18, is used for the individual elements. This structure may be represented as a geometric tetrahedron by connecting the tape spring end points with straight edges, as shown in Fig. 19.

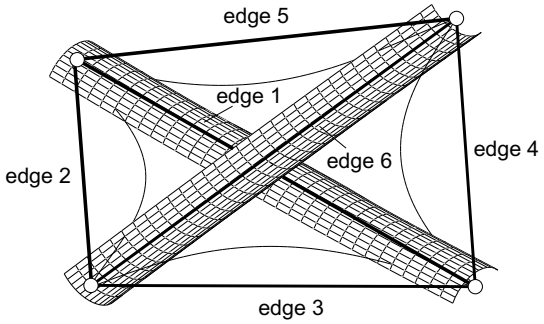

Fig. 19. Superposition of a geometric tetrahedron onto the bistable tetrahedron structure.

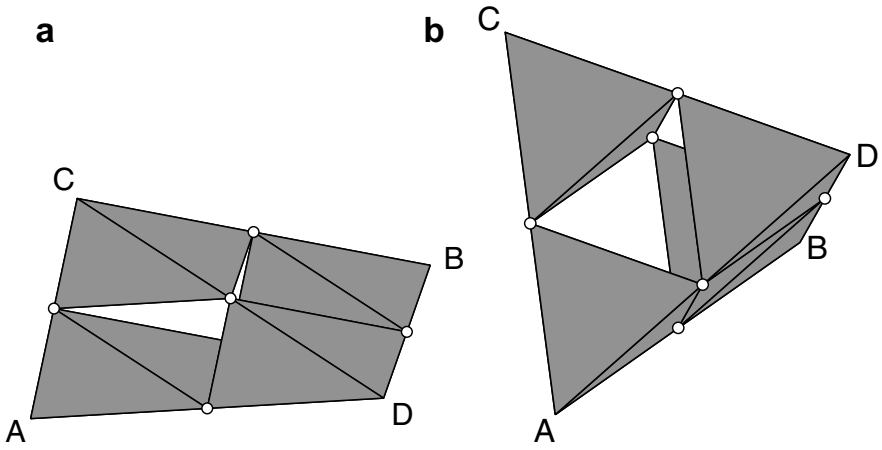

Fig. 20. The extreme configurations of a multistable super-tetrahedron consisting of four bistable tetrahedra. (a) All bistable tetrahedra in the high-energy stable configuration. (b) All bistable tetrahedra in the low-energy stable configuration.

The configurations of the multistable super-tetrahedron that are of the greatest interest are those in which either all or none of the sub-tetrahedra are actuated. The super-tetrahedron configuration in which all the sub-tetrahedra (represented as shown in Fig. 19) are in the high-energy configuration is shown in Fig. 20(a). When each bistable tetrahedron is transitioned to its low-energy stable state this may be described in terms of the changes in the edge lengths: edge 1 and edge 6 reduce their length by 25%; the remaining edges increase their length by 5.3%. The super-tetrahedron configuration in which all the sub-tetrahedra are in the high-energy configuration is shown in Fig. 20(b).

It can be seen that there is a substantial increase in height and enclosed volume between the extreme configurations – valuable properties for a deployable structure. These properties may be retained for structures with larger numbers of bistable elements provided the structural determinacy is retained. A possible technique for achieving this is to construct hierarchical systems in which a super-tetrahedron may itself be used as a sub-element in a larger super^2-tetrahedral structure, and so on. A super^n-tetrahedron in which n is large approximates a three-dimensional form of the 'Sierpiński Gasket' fractal. Fractal structures have many potential uses, including antennas (Gianvittorio and Rahmat-Samii, 2000) and turbulence control devices (Mazzi and Vassilicos, 1999).

4.2. Super-tetrahedron physical model

A physical model was constructed of the super-tetrahedron assembly introduced in the previous section to demonstrate the realisation of the idealised model in Fig. 20 into a multistable compliant mechanism. The idealised spherical joints which were assumed in the compatibility analysis were approximated by strips of single-ply triaxial-weave CFRP which act as both rotational and torsional living hinges. The constructed model has a total mass of 4 g and in the stowed configuration a total height of 2.9 cm and a projected area of 155 cm^2.

Photographs of the model may be seen in Figs. 21 and 22. The kinematic- and static-determinacy of the super-tetrahedron is illustrated by the fact that the structure can sustain any combination of individual tetrahedron elements changing their configuration without the loss of rigidity, or the addition of significant prestress (neglecting the small prestress resulting from the flexure of the living hinges).

Of especial interest in Fig. 21 are (a) and (e) which correspond to the configurations shown in Fig. 20(a) and (b), respectively. The difference in height between the stowed (all actuating tetrahedra in their high-energy configurations) and de-

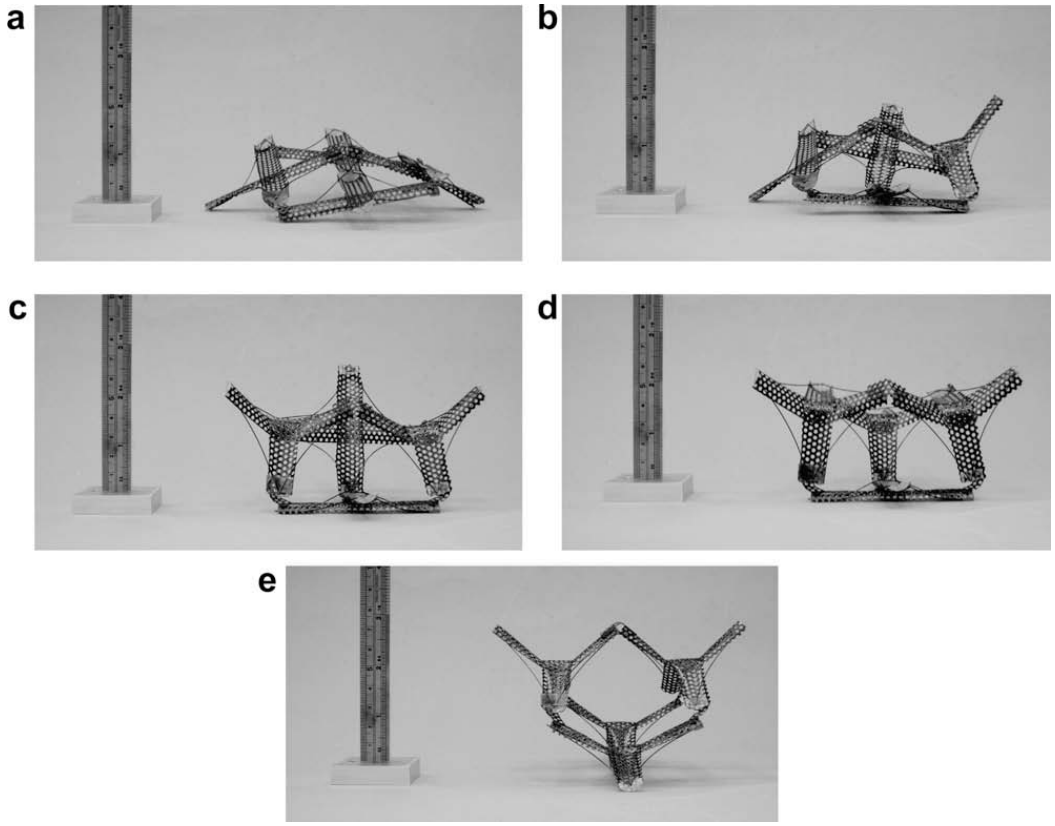

Fig. 21. Side views of the super-tetrahedron physical realisation. (a) Super-tetrahedron: fully stowed. (b) Super-tetrahedron: one tetrahedron actuated. (c) Super-tetrahedron: two tetrahedra actuated. (d) Super-tetrahedron: three tetrahedra actuated. (e) Super-tetrahedron: fully deployed.

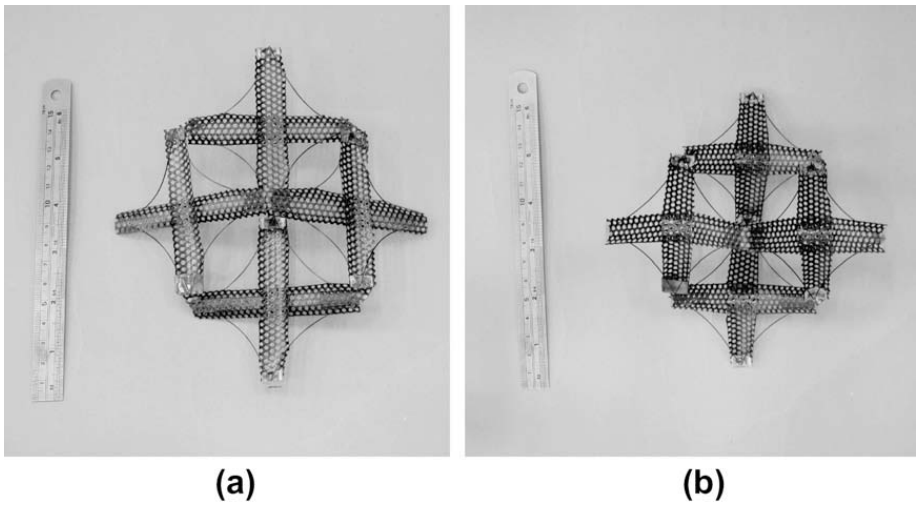

Fig. 22. Super-tetrahedron plan view, (a) fully stowed and (b) fully deployed.

ployed (all actuating tetrahedra in their low-energy configurations) is 4.1 cm corresponding to an increase of 2.2 times. The observed twist that is present in Fig. 21(a) is the result of imperfections which were introduced during fabrication of the model, which was constructed in the low-energy configuration. In Fig. 22 these same configurations are shown in plan view. The decrease in projected area from the stowed to deployed configurations is determined to be 18%.

5. Conclusions

It has been shown that it is feasible to construct compliant multistable adaptive structures that exhibit large geometric changes under actuation without the use of conventional mechanism components.

This paper has demonstrated the complete process of designing an asymmetrically-bistable tetrahedral structural element which is used as the basis of a compliant multistable structure. The resulting structure consists of four tetrahedral elements and increases its height by over 200% when all elements are changed from their high-energy to their low-energy stable state. Such a structure has potential applications for deployable components in aerospace and other fields.

The combination of linear and nonlinear springs may result in structures which are, at the very least, asymmetrically-bistable. A method for designing these structures using finite element analysis is demonstrated. It is shown to be possible, however, for additional stable states to be present, which are revealed by careful analysis. The presence of imperfections has been shown to cause buckling modes to interact, causing unexpected post-buckling paths to be followed. A design for a truly bistable compliant tetrahedral element has been proposed which utilises internal contact to remove unwanted stable states.

Acknowledgements

The work presented in this paper was funded by the Cambridge-MIT Institute (CMI) and carried out in the Department of Engineering, University of Cambridge in collaboration with Prof. Dubowsky at MIT. Two anonymous referees are thanked for their helpful comments, and for introducing the authors to the Sierpiński Gasket.

References

Chirikjian, G., 1994. A binary paradigm for robotic manipulators. Proceedings of the IEEE International Conference on Robotics and Automation 4, 3063–3069.

Dano, M.-L., Gendron, G., Picard, A., 2000. Mechanical Behavior of a Triaxially Woven Fabric Composite. Mechanics of Composite Materials and Structures 7, 207–224.

Gianvittorio, J.P., Rahmat-Samii, Y., 2000. Fractal element antennas: a compilation of configurations with novel characteristics. In: Proceedings of the IEEE Antennas and Propagation Society International Symposium, pp. 1688–1691.

Howell, L., 2001. Compliant Mechanisms, first ed. John Wiley and Sons.

Hunt, K.H., 1978. Kinematic Geometry of Mechanisms, first ed. Oxford University Press.

Mazzi, B., Vassilicos, J.C., 1999. Fractal-generated Turbulence. Journal of Fluid Mechanics 502, 65–87.

Plante, J.-S., Santer, M., Dubowsky, S., Pellegrino, S., 2005. Compliant Bistable Dielectric Elastomer Actuators for Binary Mechatronic Systems. In: Proceedings of the IDECT/CIE 2005: ASME Mechanism and Robotics Conference, DETC2005-85576.

Seffen, K., Pellegrino, S., 1999. Deployment dynamics of tape springs. Proceedings of the Royal Society of London A 455, 1003–1048.